Characterization of nanoscale cracking at the interface between virgin and aged asphalt binders based on molecular dynamics simulations

Yohannes L. Yaphary,[a] Zhen Leng,*[a] Haopeng Wang,[b] Shisong Ren,[c] and Guoyang Lu[a]

[a] Department of Civil and Environmental Engineering, The Hong Kong Polytechnic University, Hung Hom, Kowloon, Hong Kong

[b] Nottingham Transportation Engineering Centre, University of Nottingham, Nottingham, NG7 2RD, UK

[c] Section of Pavement Engineering, Faculty of Civil Engineering & Geosciences, Delft University of Technology, Stevinweg 1, 2628 CN, Delft, the Netherlands

*Correspondence should be addressed to Zhen Leng (email address: zhen.leng@polyu.edu.hk)

HIGHLIGHT

- Nanoscale crack propagation of virgin-aged binder interface was studied
- MD simulations were conducted to characterize the nanoscale crack propagation
- The interface was modeled as trilayer phases composed of virgin, virgin-aged blended and aged binders
- Simulations and experiments indicated the cracking zones at virgin-aged asphalt binder interface
- Crack initiated from the blended binder and its interface with virgin and aged binders

ABSTRACT

Low-temperature cracking is a major concern to improve the utilization of recycled asphalt mixture (RAM). A mechanism by which the crack propagates can provide a basis for advanced technological mitigation. Micro-crack formations in the interfacial proximity of the virgin and aged binders have been identified from electron microscopy tests. Atomic force microscopy (AFM) experiment showed the trilayer phases at the virgin-aged binder interface. In this study, molecular dynamics (MD) simulations were conducted to understand the nanoscopic crack propagation characteristics at the virgin-aged binder interface in the asphalt mixture with RAM. It was found that the blended binder of virgin and aged binders, and its interfaces with virgin and aged binders appeared to be the crack propagation zones. The relatively more significant matrix contraction of virgin binder and stiffer aged binder at a low temperature can cause more considerable tensile stress at the blended binder and its interfaces. Consequently, interfacial crack propagation became more profound and decreased the low-temperature cracking resistance.

GRAPHICAL ABSTRACT

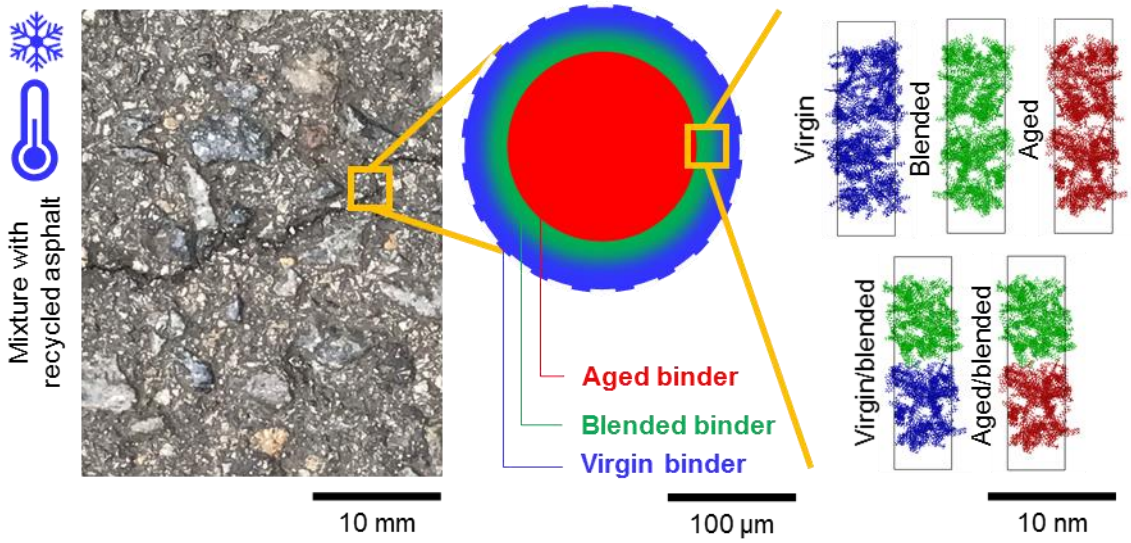

KEYWORD

Recycled asphalt mixture; Interfacial blending zone, Molecular dynamics simulations; Cracking resistance; Temperature.

1. INTRODUCTION

Petroleum asphalt cement has been widely used as the binder for mixtures utilized in infrastructure and building constructions, such as road pavements and roof shingles [1] [2]. The limited storage of crude oil worldwide promotes the optimal usage of asphalt binder from new petroleum processing [3]. On the other hand, as a compound of organic molecules, asphalt cement naturally undergoes an aging process during the construction and service [4]. At the end of service life, the massive wastes from the demolished construction structures create a classical shortage issue for landfilling. Recycled asphalt mixture (RAM) from reclaimed asphalt pavements (RAP) and shingles (RAS) has been an effective solution for an environmentally friendly and economical approach towards sustainable asphalt pavement construction [5]. Nevertheless, optimizing the RAM content into a new asphalt mixture is still challenging due to the limited fundamental understanding regarding the interaction between virgin and aged binders [6]. For instance, the RAP

content in pavement construction is typically limited to 20-25% due to the issues mainly related to the increased stiffness of the mixture [7].

The increased stiffness of the asphalt mixture containing RAM is advantageous to improve the mixture properties at a relatively high temperature (e.g., rutting resistance), but disadvantageous to the thermal cracking resistance at a low temperature (i.e., below 0 ^{o}C) [8] [9]. This disadvantage causes a hurdle for the higher recycling stem of RAM [10]. The incomplete blending of the stiffer aged binder from RAM [11] [12] [13] [14] [15] is deemed to aggravate the cracking resistance at a low temperature. And, the insight by which the stiffer aged binder from RAM drives such aggravation remains little.

The research based on electron microscopy tests has identified the micro-crack formations in the interfacial proximity of the virgin and aged binders, suggesting the inferior adhesion and weak zone for crack formation and propagation [16]. More detailed investigations by using atomic force microscopy (AFM) experiment showed the trilayer phases at the virgin-aged binder interface [17]. The interfacial blending zone existed between virgin and aged binders. This blending zone can exist from the interfacial diffusion of incompletely blended virgin-aged binders during the placing and cooling of the mixture from hot mixing to ambient temperature. The thickness (e.g., 25 to 50 μm) can vary depending on the diffusing temperature and period, and types of virgin and aged binders [17] [18] [19]. Heterogenous molecular species exist in virgin and aged binders at the nanoscale and govern their interfacial characteristics [20]. Hence, the investigation on nanoscale crack propagation at the interface between virgin and aged asphalt binders can deliver a more detailed mechanism from the reduced cracking resistance of the mixture with RAM at a relatively low temperature.

Molecular dynamics (MD) simulations have been employed as a powerful tool to study asphalt binder characteristics at the nanoscale. Li and Greenfield [21] improved the AAA-1 asphalt binder model, and the model has been widely used [22] [23] [24]. Pan et al. [25] modeled the aged asphalt binder based on Li and Greenfield's AAA-1 asphalt binder model. Studies have demonstrated the capabilities of MD simulations to gain more insight into various nanoscale characteristics of virgin and aged binders [26] [27] [28] [29]. The simulations have also been employed to study the interaction between virgin and aged binders [30]. Nevertheless, the interfacial blending zone at the interface between virgin and aged binders was not considered, and their nanoscale crack propagation has not been investigated.

The present study aims to investigate the nanoscopic crack propagation at the trilayer phases of a virgin-aged binder interface in a mixture with RAM at a relatively low and high temperature through MD simulations. The trilayer phases were modeled as three components: virgin and aged asphalt binders and a blend of them. The models of the trilayer phases were validated by comparing the simulated and experimental differences between the virgin and aged binder characteristics at different temperatures. The investigation was performed on the volumetric strain, stress-strain profile, bulk modulus , cohesive and adhesive energies and cracking mode (i.e., under pulling) of the asphalt binder models. The simulation results were then linked with the experimentally observed microscale cracking tendency at the virgin-aged binder interface. Furthermore, more detailed insight into how decreasing temperature can decline asphalt mixture cracking resistance with RAM was elaborated. The information from the present study provides a more detailed mechanism of aggravated low-temperature cracking resistance of asphalt mixture containing RAM. It can be useful in designing the treatment to alleviate the concerns of using RAM.

2. Model and simulation methods

2.1. Model

Asphalt binder is a naturally occurring compound with more than 10^5 types of organic molecules [20]. A simplified and reliable asphalt binder model has been progressively developed to understand the fundamental structure-property relationship down to the molecular scale. ASTM D4124 classified the hydrocarbons mixture of asphalt binder into four components of saturates, aromatics, resins and asphaltenes (SARA). Li and Greenfield [21] modified the previously interpreted molecular structure of asphalt binder models to obtain a closer agreement between model has good agreement with the experimental characteristics associated with AAA-1. Since then, the model of AAA-1 has been commonly used to find the behavioral insight of aged binder at the molecular scale [25] [31] [24] [32].

To construct the aged binder model, Pan et. al., [25] modified the AAA-1 binder model by Li and Greenfield [21]. The molecular structures of the aged binder were constructed according to the existing sensitive functional groups in the aromatic, resin and asphaltene molecules of the virgin binder. The molecular structures of saturates remained the same because they are not

susceptible to oxidation [33] [34] [4]. In this study, the virgin and aged binder models were developed after the modification by Pan et. al. [23]. The molecular composition of SARA components is shown in Table 1. The blended binder in Table 1 was used to develop the model to represent the blending zone. Herein, the blended binder with the virgin to aged binder ratio of 50 : 50 was used as the average composition of binder in the blending zone. Figure 1 and 2 show the molecular structures of virgin and aged binders, respectively.

Table 1. Molecular composition of a virgin, aged and blended binder.

Component	Molecule	Number of molecules (Non-oxidized/oxidized)		
		Virgin binder	Aged binder	Blended binder
Saturates	Squalane	4/0	4/0	4/0
	Hopane	4/0	4/0	4/0
Aromatics	PHPN	11/0	0/11	5/6
	DOCHN	13/0	0/13	7/6
Resins	Quinolinohopane	4/0	0/4	2/2
	Pyridinohopane	4/0	0/4	2/2
	Thioisorenieratane	4/0	0/4	2/2
	Benzobisbenzothiophene	5/0	0/5	2/3
	Trimethylbenzene-oxane	15/0	0/15	8/7
Asphaltene	Asphaltene-pyrrole	2/0	0/2	1/1
	Asphaltene-phenol	3/0	0/3	1/2
	Asphaltene-thiophene	3/0	0/3	2/1

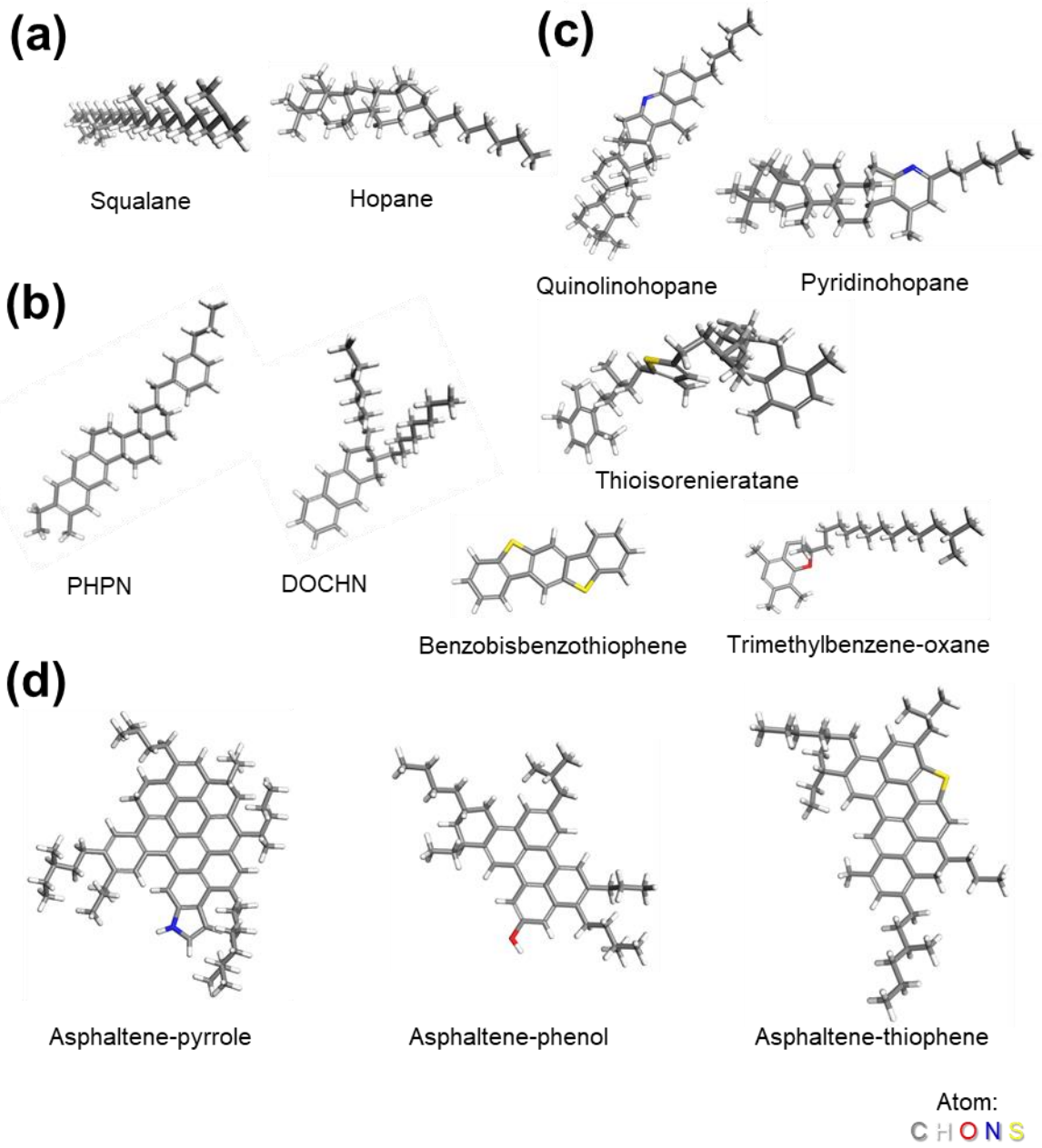

Figure 1. Molecular structures (a) saturates, (b) aromatics, (c) resins and (d) asphaltenes of virgin binder model as adopted from [21].

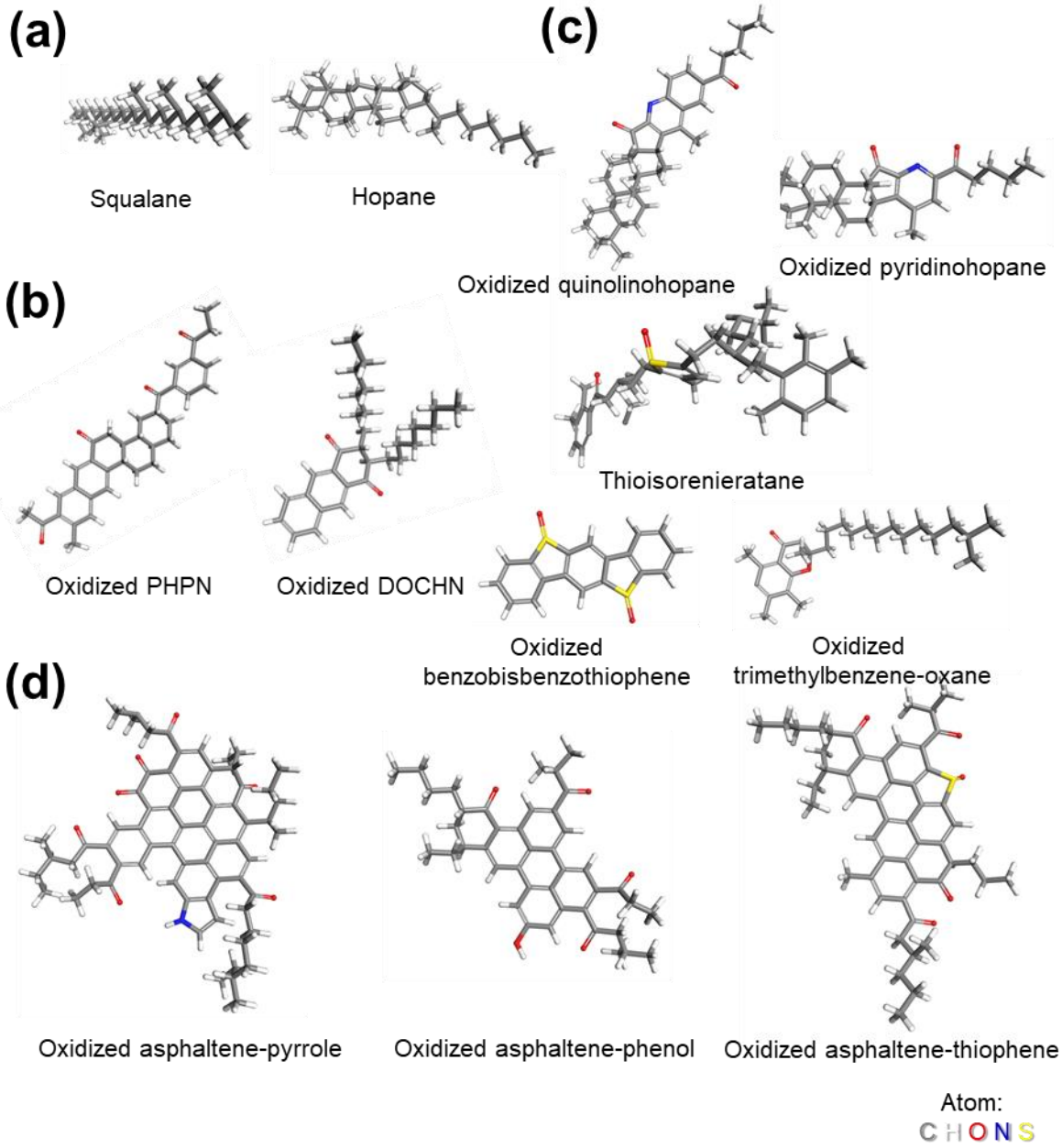

147

148 Figure 2. Molecular structures (a) saturates, (b) aromatics, (c) resins and (d) asphaltenes of aged
149 binder model as adopted from [25].

150

151 Based on the molecular composition for binders in Table 1 and their molecular structures
152 in Figures 1 and 2, two groups of simulation boxes were constructed, as seen in Figure 3. All the
153 simulation boxes had 40x40x115 $Å^{3,}$ and the binder molecules were placed at the middle region
154 with a height of 85 Å. The spaces at the bottom and top parts were left empty. The simulation box

and molecular placement were designed to accommodate different investigations, as explained in the following sections. The first group of simulation boxes consists of two virgin, blended and aged binders, as shown in Figure 3a. The molecules were randomly dispersed within a binder. In the second group of simulation boxes, the bilayer binders, composed of virgin and aged binder topped with blended binder within each simulation box, were constructed as seen in Figure 3b. The models in this figure were built according to the observed interfaces of trilayer phases of a virgin-aged binder interface from the AFM experiment, as shown in Figure 4 [17] [19].

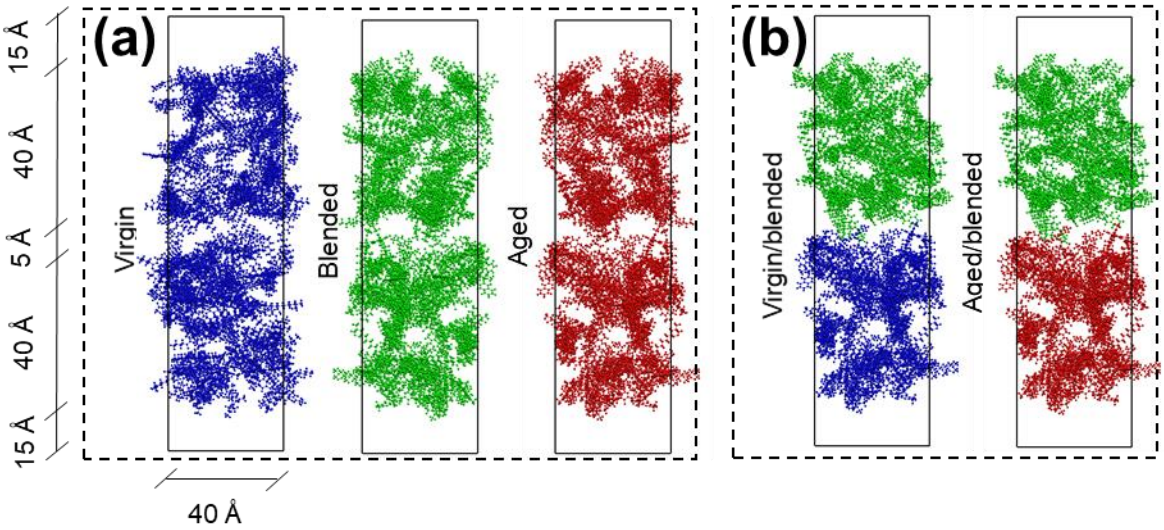

Figure 3. Initial simulation boxes of (a) the virgin, blended and aged binders and (b) virgin-blended and aged-blended binders.

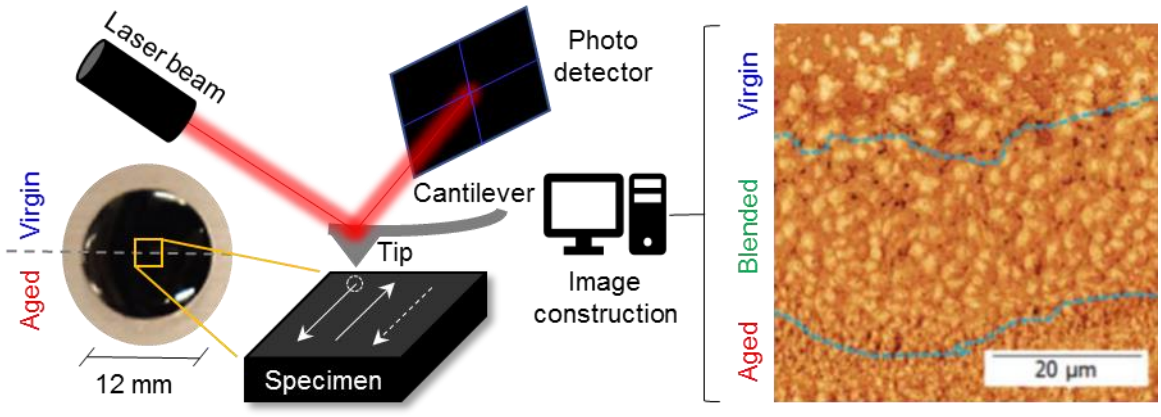

Figure 4. Image of trilayer phases of a virgin-aged binder interface obtained from AFM [17] [19]. The sample was prepared by firstly heating the virgin-aged bilayer binder. After the sample

was cooling down, the tapping mode of AFM was run (i.e., with a back-and-forth trajectory) on the area crossing the initial interface of the virgin-aged bilayer binder.

2.2. Dynamic evolution and properties

The atomic and molecular interaction was governed by employing the polymer consistent force field (PCFF) [35]. This is a class II force field that is applicable for MD simulations of asphalt binder [24] [36] [37]. MD simulations were performed using LAMMPS (Large-scale Atomic/Molecular Massively Parallel Simulator), a well-tested and widely used open-source classical molecular dynamics code [38]. Various schemes of MD simulations were performed to obtain the characteristics at different temperatures. A Nose-Hoover thermostat and barostat were used throughout the simulation to control the temperature and pressure [39]. Short-range interactions were truncated at 12 Å, and long-range electrostatic interactions were computed using the Ewald summation.

2.2.1. Mechanical properties

The binders' thermodynamic information of density, temperature and pressure was obtained from MD simulations to determine the mechanical properties (i.e., volumetric strain, ultimate tensile strength (f_u) and bulk modulus (K)) of the virgin, blended, and aged binders. These mechanical properties were compared with the experimental results to evaluate the viability of the present study's simulation scheme in capturing the effects of temperature on virgin, blended and aged binders.

MD simulations were performed under isothermal-isobaric ensemble at 1 atm and varied temperatures to investigate the thermal effect on the binders' volumetric strain. The density change (i.e., the total mass of atoms divided by the altered volume of the simulation box due to thermal effect) was employed to indicate the volumetric strain. The simulation to obtain the density was run at increasing temperatures from -170 to 230 ^{o}C with a 50 ^{o}C increment. At each temperature level, the simulations were run for 1.1 ns with a timestep of 0.1 fs. The simulation achieved the equilibrium state before 1 ns, as indicated by the steady potential energy. The averaged density was obtained through the last 0.1 ns period. Afterward, the temperatures and averaged densities were plotted, and T_g was determined as the temperature at which the linear slope changed.

The simulations of the virgin, blended, and aged binders were equilibrated at temperatures of -28, 10, -10 and 25 ^{o}C to investigate the effect of temperature on f_u. The temperature range minima of -28 ^{o}C is the minimum pavement design temperature of PG 58-28 as per ASTM D6373 [40]. The AAA-1 model is equivalent to PG58-28 [41]. The temperature range maxima of 25 ^{o}C was selected for being consistent with the room temperature used to study the characteristics of virgin-aged binder interface [16] [17] [18] [19]. At an equilibrium state, the simulation boxes were uniaxially deformed with the strain rate of 10^{-4} fs^{-1}. This strain rate was used to result in the consistent effect of temperature on binders' tensile strength between the simulation and experiment [42]. Simultaneously, the generated stresses were recorded along the axes of uniaxial deformation. The f_u was determined as the maxima of the stress-strain profile.

The investigation of bulk modulus was performed at the more focused temperatures, which are -28 and 25 ^{o}C. These temperatures were used to represent the low temperature and intermediate temperature during pavement service, at which thermal cracking and fatigue cracking may occur respectively. MD simulations were run for 1.1 ns, wherein the equilibrium state was achieved. The thermodynamic information of pressure and temperature was obtained every 0.1 fs to calculate K by using Equation 1, the method proposed by Tildesley and Allen [43]. The V, P, k_B and T are volume, pressure, Boltzmann constant and temperature, respectively. This method uses the volume fluctuations of the MD simulations run under an isothermal-isobaric ensemble to calculate K. The averaged K was obtained through the last 0.1 ns simulation period.

$$K = -V\left(\frac{\partial P}{\partial V}\right)_T = \frac{\langle V\rangle k_B T}{(\langle V^2\rangle - \langle V\rangle^2)} \quad (1)$$

2.2.2. Cohesive and adhesive energies

The calculation of cohesive and adhesive surface energy (γ_s) was performed after the equilibration process for 1.1 ns under the canonical ensemble. Herein, the definition of cohesive energy was the interfacial surface energy between two sets of molecules within the systems of the virgin, aged and blended binders. The adhesive energy was defined as the interfacial surface energy between a set of the blended binder with a set of virgin and aged binders. The γ_s was calculated by using Equation 2 where γ_{all}, γ_{bot} and γ_{top} are potential energy of all, bottom and top part of a binder as illustrated in Fig. 4. A_v is the interfacial area of Voronoi tessellation between the atoms in the bottom and top binder.

$$\gamma_s = \frac{\gamma_{all} - \gamma_{bot} - \gamma_{top}}{A_v} \quad (2)$$

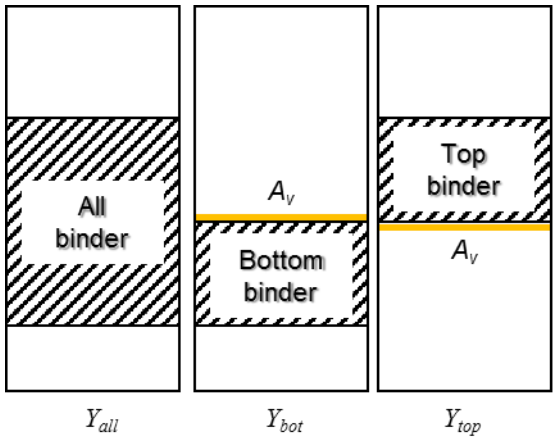

Fig. 5. Schematic representation of the potential energy calculation of all, bottom and top part of a binder (i.e., γ_{all}, γ_{bot} and γ_{top}). A_v is the interfacial area of Voronoi tessellation between the atoms in the bottom and top binder.

2.2.3. Steered molecular dynamic (SMD) simulations

Steered molecular dynamics (SMD) simulations were employed to examine the cracking modes of virgin-blended and aged-blended binders at temperatures of 25 and -28 ^{o}C. The SMD simulations were used as non-equilibrium MD simulations, which can be more relevant to simulate binder behaviors during the mixture deformation. SMD applies a steered external force to accelerate the conformational change of the investigated system along the assumed path [44]. Thus, the process (e.g., the cracking modes of virgin-blended and aged-blended binders) can be observed within the time scale that applies to MD simulations. Prior to performing SMD simulations, the simulation boxes in Figure 3b were enlarged upward. This enlargement was to provide enough space for the upward movement of a virtual spring (i.e., tethered to a part of the upper binder) so the upper binder could be pulled until the crack propagated. The pulling mode of SMD simulations was performed after the equilibration process for 1.1 ns under the canonical ensemble. The configuration used for SMD simulations is shown in Figure 6. Following the equilibration process, the fourth bottom part of the virgin and aged binder was restrained, while the fourth top part of the blended binder was rigidified and tethered with a visual spring. This

spring has a stiffness of 65 mN/m and moved upward to the height of 180 Å with a pulling speed of 0.001 Å/fs. The 65 mN/m was the cantilever stiffness of atomic force microscopy (AFM) used to study adhesion appropriately [45]. SMD adopt a similar concept with AFM [45] [46]. The height of 180 Å was set to create enough moving space for the virtual spring to separate the virgin-blended and aged-blended binders into two parts. The 0.001 Å/fs was the value chosen within the range of commonly used pulling speeds for SMD simulations [47] [48].

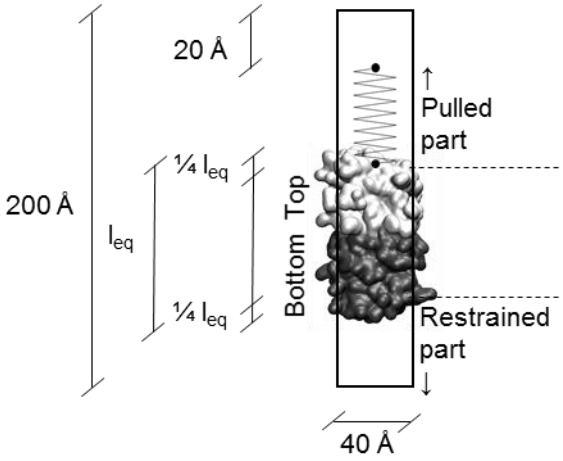

Figure 6. Schematic representation of the configuration used for the steered molecular dynamics (SMD) simulations of the virgin-blended and aged-blended binders (i.e., represented by bottom and top parts). The total equilibrium height (l_{eq}) of binders was ~ 80 Å. The fourth bottom part of the virgin and aged binder was restrained. The virtual spring of SMD was tethered at the fourth top part of the blended binder.

3. RESULTS AND DISCUSSION

3.1. Density, glass transition temperature and volumetric strain

Figure 7 shows the higher densities of the aged binder than the virgin binder at different temperatures. This changing trend on density is consistent with the experimental observation [49]. The change in gradient of temperature-density plot have been associated to the glass transition temperature (T_g) [50] [31]. It is defined as a temperature at which the asphalt changes from the viscoelastic state to the glassy state and vice versa [51]. The latter state occurs below T_g. The glass temperatures (T_g) of binders in Figure 7 were between ± 25 ^{o}C. This range agrees with the

experimental values reported from previous studies with most Tg of different binders were below -10 °C [52] [53] [54]. Determined T_g was influenced by the binder composition and used measuring technique [55].

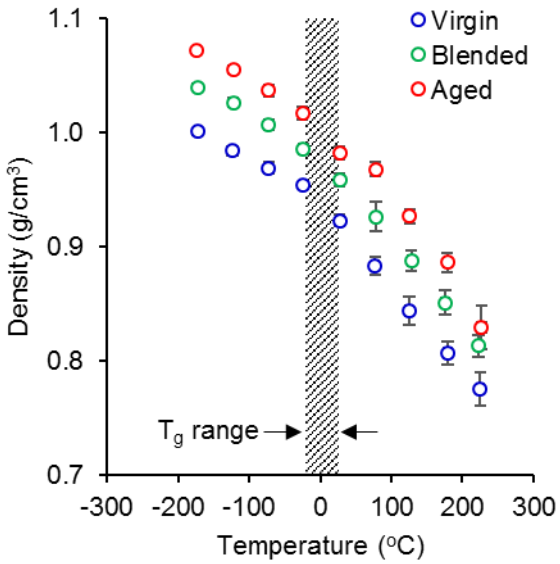

Figure 7. Density of the virgin, blended and aged binders at different temperatures. T_g is the transition glass temperature in the range of ± 25 °C.

It should be noted that the densities shown in Figure 7 were obtained from MD simulations performed under an isothermal-isobaric ensemble wherein the masses of simulation boxes were kept constant by maintaining the number of atoms. Therefore, the density changes were merely due to the binders' volumetric strain. The thermal contractions among the binders could also be compared based on the density changes. Figure 8 shows the volumetric thermal contraction of binders from 25 to -28 °C, indicating the higher volumetric thermal contraction of virgin binders than those of blended and aged binders. The higher volumetric thermal contraction of virgin binder was in line with the indication that the less stiff binder at low temperature would undergo more volumetric thermal contraction [7].

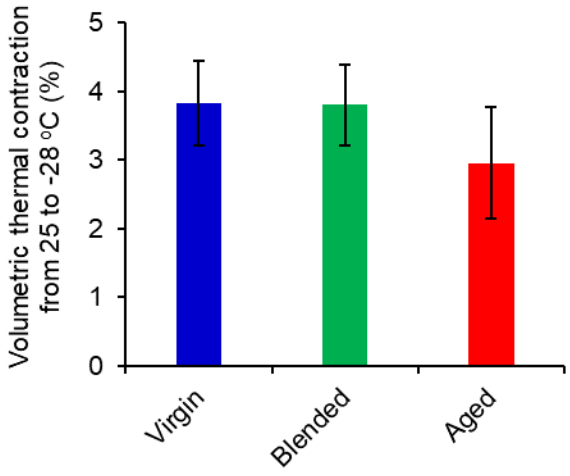

Figure 8. Volumetric thermal contraction from 25 to -28 °C.

3.2. Ultimate stress and bulk modulus

Figure 9 and 10 show the stress-strain profile and f_u of binders from 25 to -28 °C. The stress-strain profiles are similar to the virgin binder from MD simulation investigated in the previous study [56]. However, the f_u were greater than the typical values obtained from the macroscopic experiment [42], which was believed to originate from the discrepancy of time scale between MD simulations and macroscopic experiment [56]. Nevertheless, the f_u of virgin binder resulted in the present study is about half the f_u obtained from the simulations in the previous study [56]. Hence, the f_u from the simulations performed in the present study is closer to the experimental values [42]. Moreover, the f_u of aged binder was higher than that of virgin binder, consistent with the experimental observation [42]. The increased f_u of binders at a lower temperature also agrees with the experimental result [42]. The effect of lowering the temperature on increasing f_u could be attributed to the closer interatomic distances indicated by the binders' volume contractions and improved densities. An atom is bound stronger with neighboring atoms when getting closer to each other.

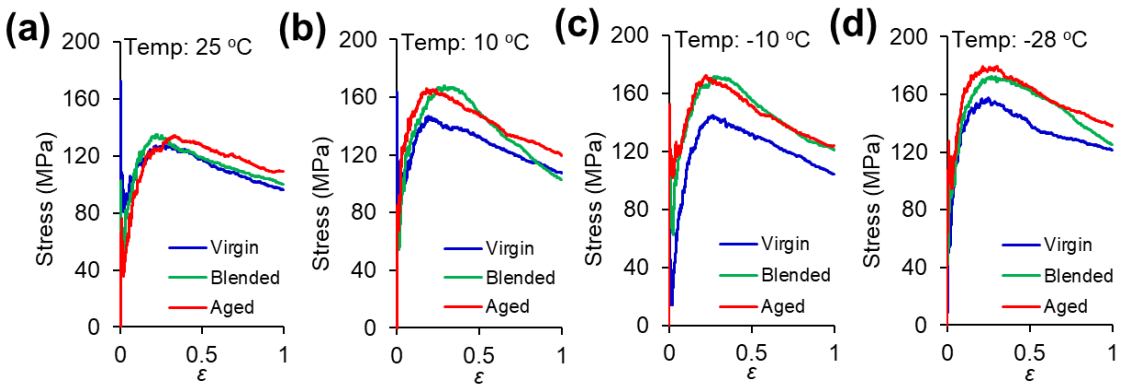

Figure 9. Stress-strain profile of binders at (a) 25 (b) 10 (c) -10 and (d) -28 °C.

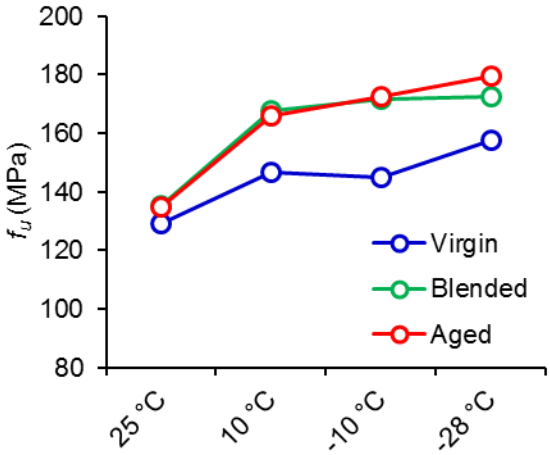

Figure 10. Ultimate stress (f_u) of binders at different temperatures.

Figure 11 shows the bulk modulus of binders. At an intermediate temperature of 25 °C, the bulk modulus increased from virgin, blended to aged binder. This increasing trend is consistent with the findings from atomic force microscopy (AFM) on the improving reduced modulus from virgin to aged binder at the virgin-aged binder interface [18]. At a low temperature of -28 °C, the lower bulk modulus of blended binder than those of virgin and aged binders was observed. It is implied that the increasing trend of bulk modulus from virgin, blended to aged asphalt might change at a lower temperature. The reversed viscosity ranking of different binders from a higher to lower temperature has also been observed experimentally [57]. This change might occur due to different molecular interactions and motions of asphalt with distinct compositions in reacting to the thermal effect [58] [59].

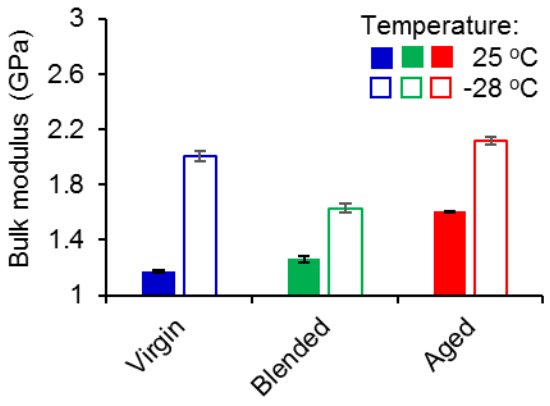

Figure 11. Bulk modulus of binders at 25 and -28 °C.

3.3. Cohesive and adhesive energies

Figure 12a shows the cohesive energies of virgin, blended and aged binders and Figure 12b presents the adhesive energies between blended binder and virgin and aged binders. It can be seen that the cohesive and adhesive energy overall increased at a lower temperature. The Wilhelmy Plate (WP) test results showed that binder's cohesive free energy increased with a decrease in temperature [60]. The higher cohesive and adhesive energies at a lower temperature could be attributed to the closer interatomic distances indicated by the binders' volume contractions and improved densities.

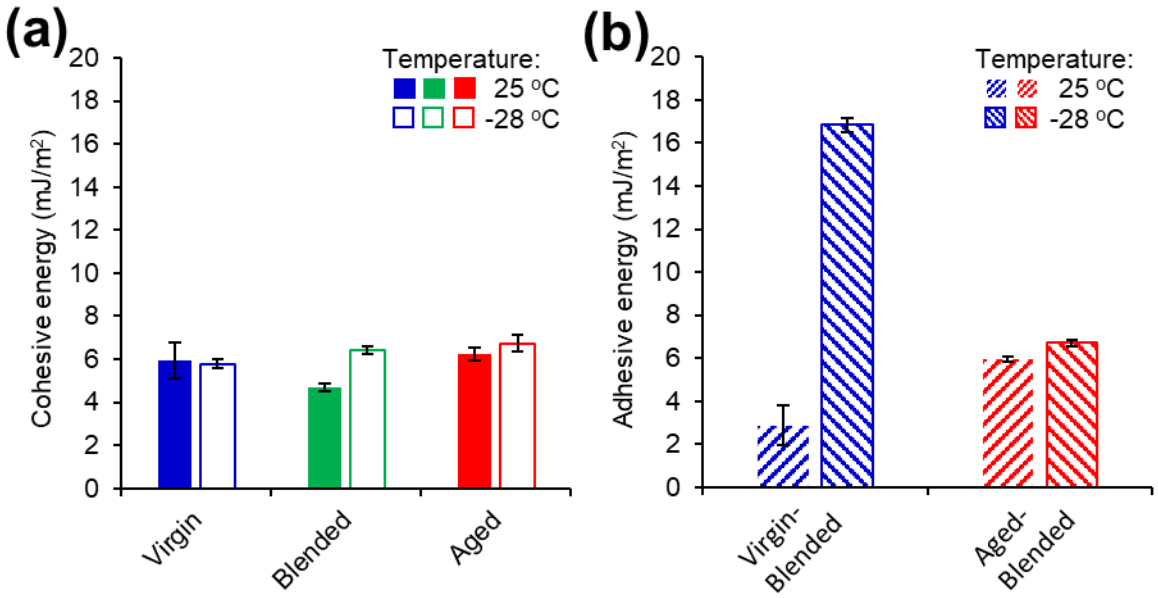

Figure 12. (a) Cohesive and (b) adhesive energy at 25 and -28 ^{o}C.

3.4. Nanoscopic cracking mode of mixture with a recycled binder

The MD simulations presented in previous sections showed the characteristic changes of binders from an intermediate to a low temperature. The investigated characteristic changes included volumetric strain, f_u, K and cohesive and adhesive energies of virgin, blended, aged, virgin-blended and aged-blended binders. The changes were consistent with the experimental reports in the existing literature. This consistency shows the viability of MD simulations scheme performed in the present study to capture the effect of temperature change on binder characteristics. It should be noted that such characteristics were obtained from the equilibrium stage of MD simulations (i.e., except stress-strain profile and f_u). The equilibrium MD simulations may not be relevant to investigate the binder behaviors during mixture deformation. On the other hand, the examination from non-equilibrium MD simulations (i.e., SMD simulations) can be more relevant to investigate binders' molecular dynamic conformation during the deformation.

In this section, the results from SMD simulations were examined to obtain insight from the interfacial cracking mode of bilayer binders under pulling. Figure 13 shows the interfacial cracking mode between blended binder and virgin and aged binders at 25 ^{o}C. The occurrence of a specific mode (i.e., 1, 2 or 3) depended on the deformation distance of the virtual pulling spring as indicated by the grey upward arrow. The crack propagation started with mode 1 caused by a relatively small deformation. In mode 1, virgin, blended and aged binders yielded at the interfaces between blended binder and virgin and aged binders. Increasing the deformation distance of the virtual pulling spring turned the mode 1 into mode 2, which was indicated by the complete fracture at the interfaces. Afterward, the crack could be transferred to the blended zone (i.e., cracking mode 3). It should be noted that the cracking modes herein referred to the localized nanoscale crack of a bulk system of binders seen from a larger scale. Additionally, the cracking mode 3 could also be attributed to the self-healing capability of the blended binders and could occur relying on the size of the crack opening. It was observed that the blended binder and its interfaces (i.e., with virgin and aged binders) appeared as weak zones. This observation agreed with the experimentally observed microscale cracking tendency that occurred at the virgin-aged binder interface as observed in a previous study [16]. The nanoscale crack propagation from SMD simulation

indicated that such microscale cracking tendency originated from the weak blended binder and its interfaces with virgin and aged binders.

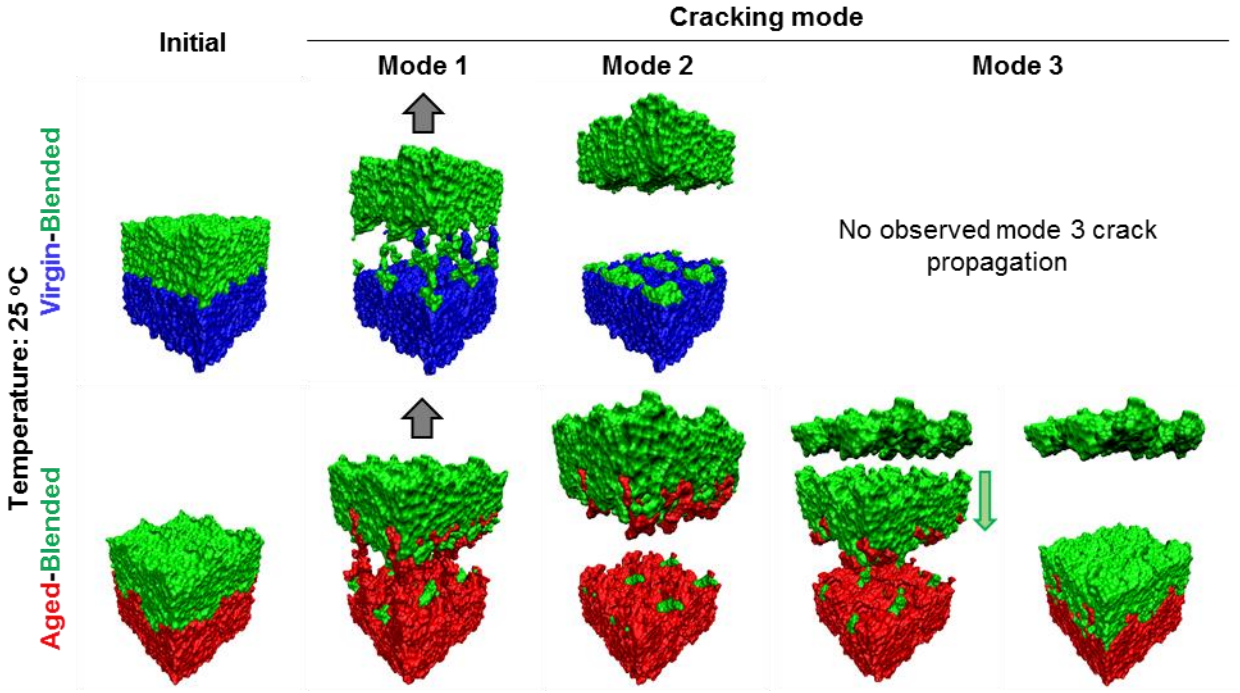

Figure 13. Interfacial cracking mode of the blended binder and virgin and aged binders at 25 °C. The grey upward arrows show the deforming direction of the tethered virtual spring and green downward arrow indicates the backward movement of detached blended binder.

At a low temperature of -28 °C, the cracking modes also occurred at the interfaces between blended binder and virgin and aged binders, as shown in Figure 14. However, it can be seen from cracking mode 1 that the aged binder remained relatively intact (i.e., compared to the observed yielding of aged asphalt during SMD simulations at 25 °C) and no observed crack propagation at the aged binder in mode 2. The increasing stiffness could cause the relatively intact aged asphalt at a lower temperature. This observation affirmed that, at a lower temperature, the stiffer aged binder plays a role in causing the aggravating cracking resistance of the mixture with RAM [7]. Based on the observations of cracking modes from SMD simulations, more detailed insight into the aggravating cracking resistance mechanism is elaborated in the following section.

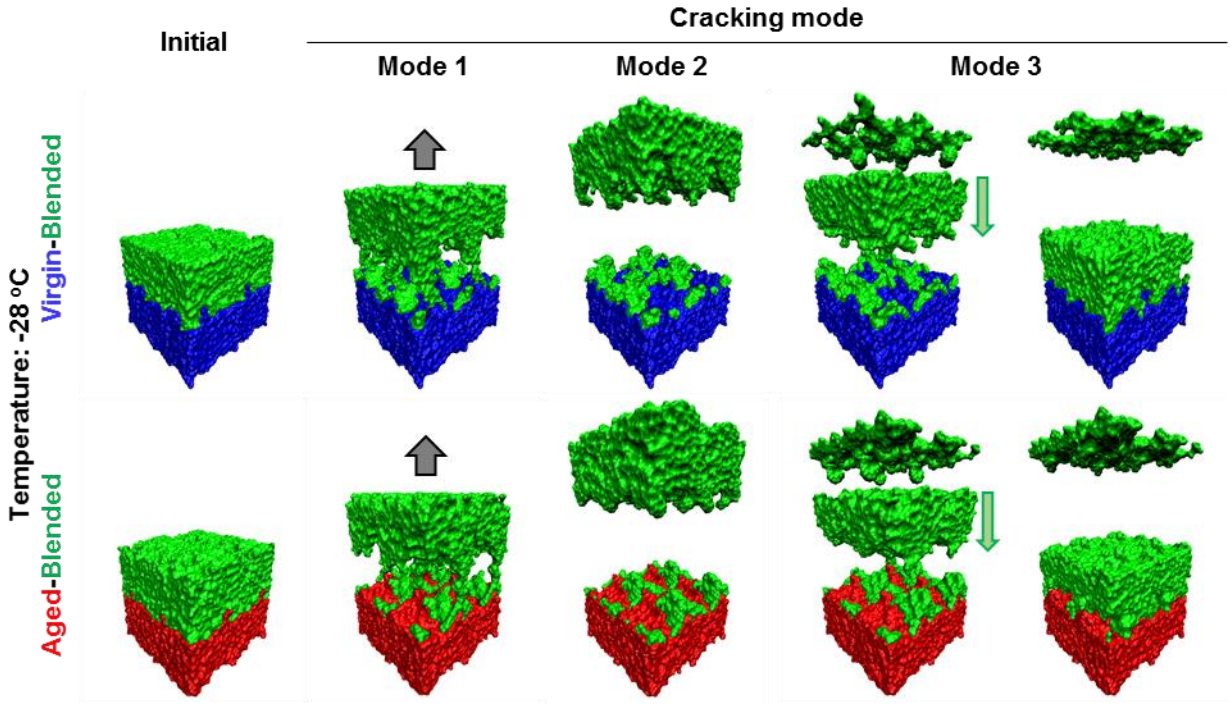

Figure 14. Interfacial cracking mode of the blended binder and virgin and aged binders at -28 °C. The meanings of grey upward and green downward arrows are the same as those described in Figure 13.

3.5. Insight from MD simulations on aggravated low-temperature cracking resistance

The cracking modes from SMD simulations implied that the larger volumetric thermal contraction of virgin binder and stiffer aged binder generated from decreasing temperature caused the aggravated low-temperature cracking resistance of asphalt mixture containing RAM. When the temperature was decreasing and under internal restrain of the asphalt mixture, the larger contraction of virgin binder and the stiffer aged binder induced more considerable tensile stress at the blended binder and its interfaces with virgin and aged binders. Consequently, the nanoscale crack propagation became more profound. The nanoscale crack could lead to micro and macroscale cracks and debond the binder at a larger scale.

The insight about the cause of the aggravated low-temperature cracking resistance of asphalt mixture containing RAM can provide a theoretical basis to develop the mitigation strategy

for the low-temperature crack. The successful mitigation strategy can improve the durability and ecological aspect of different asphalt-based construction and building materials containing RAM. Cracking binder can be a path for surface water to enter the internal structure of asphalt pavement and lead to water damages [61]. In other applications, the cracking binder can cause disfunction of waterproofing materials (e.g., roof shingle and surface applied membrane for bridge decks and flat roofs) and need for replacement.

For instance, the reduced stiffness of the aged binder by incorporating rejuvenator combined with the less stiff virgin binder [62] [63] can be a proper strategy to improve the low-temperature cracking resistance of the mixture with RAM. This strategy's mechanism can mainly come from the more elastic elongation of the binders to accommodate the thermal deformation caused by decreasing temperature. Simultaneously, the interfacial tensile stresses can be reduced. Furthermore, the more effective design should consider the diffusion rate between virgin and aged binder so the thickness of blended binder can be predicted and the location of the interface can be estimated. This information can be useful in selecting fiber specifications to effectively bridge the propagated crack within the range that the self-healing of binders can occur.

3.6. Recommendation for future study

The investigation on the nanoscale crack propagations between blended binder and virgin and aged binders has provided a more detailed mechanism by which the low-temperature cracking resistance of asphalt mixture containing RAM is aggravated. More studies can be performed in the future to advance further the mechanism, such as:

- The molecular diffusion crossing the interface between virgin and aged binders. This study can provide a more realistic binder composition at the interfacial blending zone, not revealed from the previous diffusion study of virgin-aged bilayer models [30]. It can be challenging due to the short timescale of MD simulations [64]. Different accelerated MD simulations [65] can be evaluated for being used.
- The nanoscale-characteristic difference at the interface between virgin and aged binder from different types and sources. Depending on the aging agents and type and source of virgin binder, the aging process can involve fragmentation, oxidation and condensation of hydrocarbons [66]. The result from the present study was limited to the aged binder from the oxidized molecules of the virgin binder.

- A qualitative and quantitative study investigating a more detailed effect of temperature (i.e., wide temperature range with smaller intervals) on the nanoscale degradation at the interfacial proximity between virgin and aged binders.

4. SUMMARY AND FINDINGS

In this study, molecular dynamics (MD) simulations have been performed to obtain a more fundamental insight on nanoscopic crack propagation of the trilayer phases of a virgin-aged binder interface in a mixture with RAM at a relatively low and high temperature. The comparison between virgin and aged binders characteristics (i.e., volumetric strain, ultimate tensile strength, bulk modulus and cohesive and adhesive energies) at different temperatures from MD simulations and experiments were overall consistent. This consistency demonstrated the viabilities of simulation schemes used in the present study to capture the thermal effect on binder characteristics.

To study the nanoscopic crack propagation of the trilayer phases of a virgin-aged binder interface, steered molecular dynamics (SMD) simulations were performed. These simulations were conducted at 25 and -28 ^{o}C to represent an intermediate and a low temperature. SMD simulations were employed to capture the molecular dynamic conformation of binders under pulling deformation. The following findings were obtained:

- The nanoscopic crack propagation mode of virgin-aged binder interface occurred likely at the blended binder and its interfaces with virgin and aged binders. This nanoscopic crack propagation mode agreed with the experimental observation, which showed that the microscopic cracking tended to occur at the virgin-aged binder interface. The observation from SMD simulations suggested that the microscale cracking tendency of virgin-aged binder interface originated from the nanoscopic crack propagation of blended binder and its interfaces.
- At a relatively low temperature, the aged binder was observed to be more intact in response to the pulling deformation. The more intact aged binder could be attributed to the stiffening aged binder caused by the temperature drop. The stiffer aged binder was less deformable and restrained more the thermal contraction of the virgin binder. Consequently, considerable tensile stress at the blended binder and its interfaces with virgin and aged binders could be built up higher, resulting in more profound interfacial crack propagation.

The information from the present study provides insight into the design strategy of the treatment for improving the thermal cracking performance of the mixture with RAM at a low temperature. The primary mechanism of the treatment is to minimize the generated tensile stress at blended binder and its interfaces with virgin and aged binders. An example of ideal treatment is to adequately lessen the stiffness of aged binder (e.g., using rejuvenator) combined with properly selected fiber specification. The less stiff aged binder can accommodate the thermal contraction of virgin binder, so the stresses of blended binder and its interfaces are minimized. Moreover, the proper use of fiber (i.e., covering the interfaces between blended binder and virgin and aged binders) can prevent the large crack propagation, allowing the self-healing process of the binders. The successful treatment can reduce the drawback from using RAM and increase its application, which is environmentally beneficial for producing asphaltic materials.

REFERENCE

1. Hung, A. and E.H. Fini, *Surface Morphology and Chemical Mapping of UV-Aged Thin Films of Bitumen.* ACS Sustainable Chemistry & Engineering, 2020. **8**(31): p. 11764-11771.
2. Gong, J., et al., *Laboratory evaluation of warm-mix epoxy SBS modified asphalt binders containing Sasobit.* Journal of Building Engineering, 2020. **32**: p. 101550.
3. Zhang, R., et al., *The impact of bio-oil as rejuvenator for aged asphalt binder.* Construction and Building Materials, 2019. **196**: p. 134-143.
4. Petersen, J.C., *Chemical composition of asphalt as related to asphalt durability*, in *Developments in petroleum science*. 2000, Elsevier. p. 363-399.
5. Yan, C., W. Huang, and Q. Lv, *Study on bond properties between RAP aggregates and virgin asphalt using Binder Bond Strength test and Fourier Transform Infrared spectroscopy.* Construction and Building Materials, 2016. **124**: p. 1-10.
6. Sreeram, A., et al., *Fundamental investigation of the interaction mechanism between new and aged binders in binder blends.* International Journal of Pavement Engineering, 2020: p. 1-11.
7. Stimilli, A., et al., *Low-temperature mechanics of hot recycled mixtures through asphalt thermal cracking analyzer (ATCA).* Construction and Building Materials, 2015. **84**: p. 54-65.
8. Xiao, F., et al., *Low temperature performance characteristics of reclaimed asphalt pavement (RAP) mortars with virgin and aged soft binders.* Applied Sciences, 2017. **7**(3): p. 304.
9. Yousefi, A.A., et al., *Cracking Properties of Warm Mix Asphalts Containing Reclaimed Asphalt Pavement and Recycling Agents under Different Loading Modes.* Construction and Building Materials, 2021. **300**: p. 124130.

10. Zaumanis, M., et al., *Influence of six rejuvenators on the performance properties of Reclaimed Asphalt Pavement (RAP) binder and 100% recycled asphalt mixtures.* Construction and Building Materials, 2014. **71**: p. 538-550.
11. Huang, B., et al., *Laboratory investigation of mixing hot-mix asphalt with reclaimed asphalt pavement.* Transportation Research Record, 2005. **1929**(1): p. 37-45.
12. Bowers, B.F., et al., *Investigation of reclaimed asphalt pavement blending efficiency through GPC and FTIR.* Construction and building materials, 2014. **50**: p. 517-523.
13. Zhao, S., et al., *Laboratory performance evaluation of warm-mix asphalt containing high percentages of reclaimed asphalt pavement.* Transportation research record, 2012. **2294**(1): p. 98-105.
14. Zhao, S., et al., *Characterizing rheological properties of binder and blending efficiency of asphalt paving mixtures containing RAS through GPC.* Journal of Materials in Civil Engineering, 2014. **26**(5): p. 941-946.
15. Sreeram, A. and Z. Leng, *Variability of rap binder mobilisation in hot mix asphalt mixtures.* Construction and Building Materials, 2019. **201**: p. 502-509.
16. Rinaldini, E., et al., *Investigating the blending of reclaimed asphalt with virgin materials using rheology, electron microscopy and computer tomography.* Composites Part B: Engineering, 2014. **67**: p. 579-587.
17. Nahar, S., et al., *First observation of blending-zone morphology at interface of reclaimed asphalt binder and virgin bitumen.* Transportation research record, 2013. **2370**(1): p. 1-9.
18. AbuQtaish, L., et al., *AFM-based approach to study blending between RAP and virgin asphalt binders.* Journal of Materials in Civil Engineering, 2018. **30**(3): p. 04017300.
19. Zhao, S., et al., *Investigation on the microstructure of recycled asphalt shingle binder and its blending with virgin bitumen.* Road Materials and Pavement Design, 2015. **16**(sup1): p. 21-38.
20. Wiehe, I. and K. Liang, *Asphaltenes, resins, and other petroleum macromolecules.* Fluid Phase Equilibria, 1996. **117**(1-2): p. 201-210.
21. Li, D.D. and M.L. Greenfield, *Chemical compositions of improved model asphalt systems for molecular simulations.* Fuel, 2014. **115**: p. 347-356.
22. Xu, G. and H. Wang, *Study of cohesion and adhesion properties of asphalt concrete with molecular dynamics simulation.* Computational Materials Science, 2016. **112**: p. 161-169.
23. Khabaz, F. and R. Khare, *Molecular simulations of asphalt rheology: Application of time–temperature superposition principle.* Journal of Rheology, 2018. **62**(4): p. 941-954.
24. Sun, W. and H. Wang, *Moisture effect on nanostructure and adhesion energy of asphalt on aggregate surface: A molecular dynamics study.* Applied Surface Science, 2020. **510**: p. 145435.
25. Pan, J., M.I. Hossain, and R.A. Tarefder, *Temperature and moisture impacts on asphalt before and after oxidative aging using molecular dynamics simulations.* Journal of Nanomechanics and Micromechanics, 2017. **7**(4): p. 04017018.
26. Guo, M., et al., *Using atomic force microscopy and molecular dynamics simulation to investigate the asphalt micro properties.* International Journal of Pavement Research and Technology, 2018. **11**(4): p. 321-326.
27. Xu, G., H. Wang, and W. Sun, *Molecular dynamics study of rejuvenator effect on RAP binder: Diffusion behavior and molecular structure.* Construction and Building Materials, 2018. **158**: p. 1046-1054.

28. Chen, Z., et al., *Performance characteristics of asphalt materials based on molecular dynamics simulation–A review.* Construction and Building Materials, 2018. **189**: p. 695-710.
29. Xu, G. and H. Wang, *Diffusion and interaction mechanism of rejuvenating agent with virgin and recycled asphalt binder: A molecular dynamics study.* Molecular Simulation, 2018. **44**(17): p. 1433-1443.
30. Ding, Y., et al., *Use of molecular dynamics to investigate diffusion between virgin and aged asphalt binders.* Fuel, 2016. **174**: p. 267-273.
31. Fallah, F., et al., *Molecular dynamics modeling and simulation of bituminous binder chemical aging due to variation of oxidation level and saturate-aromatic-resin-asphaltene fraction.* Fuel, 2019. **237**: p. 71-80.
32. Yang, Y., et al., *Reactive molecular dynamic investigation of the oxidative aging impact on asphalt.* Construction and Building Materials, 2021. **279**: p. 121298.
33. Corbett, L. and R. Merz, *Asphalt binder hardening in the Michigan Test Road after 18 years of service.* Transportation Research Record, 1975(544).
34. Pan, T., Y. Lu, and S. Lloyd, *Quantum-Chemistry Study of Asphalt Oxidative Aging: An XPS-Aided Analysis.* Industrial & Engineering Chemistry Research, 2012. **51**(23): p. 7957-7966.
35. Sun, H., et al., *An ab initio CFF93 all-atom force field for polycarbonates.* Journal of the American Chemical Society, 1994. **116**(7): p. 2978-2987.
36. Gao, Y., et al., *Impact of minerals and water on bitumen-mineral adhesion and debonding behaviours using molecular dynamics simulations.* Construction and Building Materials, 2018. **171**: p. 214-222.
37. Xu, M., et al., *Improved chemical system for molecular simulations of asphalt.* Energy & Fuels, 2019. **33**(4): p. 3187-3198.
38. Plimpton, S., *Fast parallel algorithms for short-range molecular dynamics.* Journal of computational physics, 1995. **117**(1): p. 1-19.
39. Evans, D.J. and B.L. Holian, *The nose–hoover thermostat.* The Journal of chemical physics, 1985. **83**(8): p. 4069-4074.
40. Yu, X., et al., *Characterization of the effect of foaming water content on the performance of foamed crumb rubber modified asphalt.* Construction and Building Materials, 2014. **67**: p. 279-284.
41. Jones, D.R., *SHRP materials reference library: Asphalt cements: A concise data compilation*. Vol. 1. 1993: Strategic Highway Research Program, National Research Council Washington, DC.
42. Cai, J., et al., *Investigation on the cohesion and adhesion behavior of high-viscosity asphalt binders by bonding tensile testing apparatus.* Construction and Building Materials, 2020. **261**: p. 120011.
43. Allen, M.P. and D.J. Tildesley, *Computer simulation of liquids*. 2017: Oxford university press.
44. Israelewitz, B., M. Gao, and K. Schulten, *Reconstructing potential energy functions from simulated force-induced unbinding processes.* Curr. Opin. Struct. Biol, 2001. **11**: p. 224-230.
45. Mikulska-Ruminska, K., et al., *Nanomechanics of multidomain neuronal cell adhesion protein contactin revealed by single molecule AFM and SMD.* Scientific reports, 2017. **7**(1): p. 1-11.

46. Yaphary, Y.L., et al., *Molecular dynamics simulations on adhesion of epoxy-silica interface in salt environment.* Composites Part B: Engineering, 2017. **131**: p. 165-172.
47. Krammer, A., et al., *Forced unfolding of the fibronectin type III module reveals a tensile molecular recognition switch.* Proceedings of the National Academy of Sciences, 1999. **96**(4): p. 1351-1356.
48. Zhang, D., U. Chippada, and K. Jordan, *Effect of the structural water on the mechanical properties of collagen-like microfibrils: a molecular dynamics study.* Annals of biomedical engineering, 2007. **35**(7): p. 1216-1230.
49. Robertson, R.E., et al., *Fundamental properties of asphalts and modified asphalts, volume I: Interpretive report*. 2001.
50. Nie, F., W. Jian, and D. Lau, *An atomistic study on the thermomechanical properties of graphene and functionalized graphene sheets modified asphalt.* Carbon, 2021.
51. Liu, J., et al., *Using the viscoelastic parameters to estimate the glass transition temperature of asphalt binders.* Construction and Building Materials, 2017. **153**: p. 908-917.
52. Usmani, A., *Asphalt science and technology*. 1997: CRC Press.
53. Anderson, D.A. and M.O. Marasteanu, *Physical hardening of asphalt binders relative to their glass transition temperatures.* Transportation Research Record, 1999. **1661**(1): p. 27-34.
54. Kriz, P., J. Stastna, and L. Zanzotto, *Glass transition and phase stability in asphalt binders.* Road Materials and Pavement Design, 2008. **9**(sup1): p. 37-65.
55. Laukkanen, O.-V., *Rheology of complex glass-forming liquids.* 2018.
56. Sun, W. and H. Wang, *Self-healing of asphalt binder with cohesive failure: Insights from molecular dynamics simulation.* Construction and Building Materials, 2020. **262**: p. 120538.
57. Anderson, D., et al., *Binder characterization and evaluation. SHRP A-369.* Washington, DC: Transportation Research Board, 1994.
58. Luo, L., L. Chu, and T. Fwa, *Molecular dynamics analysis of oxidative aging effects on thermodynamic and interfacial bonding properties of asphalt mixtures.* Construction and Building Materials, 2021. **269**: p. 121299.
59. Hu, K., et al., *Mechanistic study of graphene reinforcement of rheological performance of recycled polyethylene modified asphalt: A new observation from molecular dynamics simulation.* Construction and Building Materials, 2022. **320**: p. 126263.
60. Cong, L., et al., *Evaluation of fatigue cracking in asphalt mixtures based on surface energy.* Journal of Materials in Civil Engineering, 2017. **29**(3): p. D4015003.
61. Wang, W., et al., *A review and perspective for research on moisture damage in asphalt pavement induced by dynamic pore water pressure.* Construction and Building Materials, 2019. **204**: p. 631-642.
62. Elkashef, M. and R.C. Williams, *Improving fatigue and low temperature performance of 100% RAP mixtures using a soybean-derived rejuvenator.* Construction and Building materials, 2017. **151**: p. 345-352.
63. Elkashef, M., R.C. Williams, and E. Cochran, *Investigation of fatigue and thermal cracking behavior of rejuvenated reclaimed asphalt pavement binders and mixtures.* International Journal of Fatigue, 2018. **108**: p. 90-95.

64. Kelchner, C.L. and A.E. DePristo, *Molecular dynamics simulations of multilayer homoepitaxial thin film growth in the diffusion-limited regime.* Surface science, 1997. **393**(1-3): p. 72-84.
65. Perez, D., et al., *Accelerated molecular dynamics methods: introduction and recent developments.* Annual Reports in computational chemistry, 2009. **5**: p. 79-98.
66. Das, P.K., et al., *On the oxidative ageing mechanism and its effect on asphalt mixtures morphology.* Materials and Structures, 2015. **48**(10): p. 3113-3127.